

Experimental implementation of encoded logical qubit operations in a perfect quantum error correcting code

Jingfu Zhang¹, Raymond Laflamme^{2,3}, and Dieter Suter¹

¹Fakultät Physik, Technische Universität Dortmund,
D-44221 Dortmund, Germany

²*Institute for Quantum Computing and Department of Physics,
University of Waterloo, Waterloo, Ontario, Canada N2L 3G1*

³*Perimeter Institute for Theoretical Physics, Waterloo, Ontario, N2J 2W9, Canada*

(Dated: November 1, 2018)

Abstract

Large-scale universal quantum computing requires the implementation of quantum error correction (QEC). While the implementation of QEC has already been demonstrated for quantum memories, reliable quantum computing requires also the application of nontrivial logical gate operations to the encoded qubits. Here, we present examples of such operations by implementing, in addition to the identity operation, the NOT and the Hadamard gate to a logical qubit encoded in a five qubit system that allows correction of arbitrary single qubit errors. We perform quantum process tomography of the encoded gate operations, demonstrate the successful correction of all possible single qubit errors and measure the fidelity of the encoded logical gate operations.

PACS numbers: 03.67.Pp, 03.67.Lx

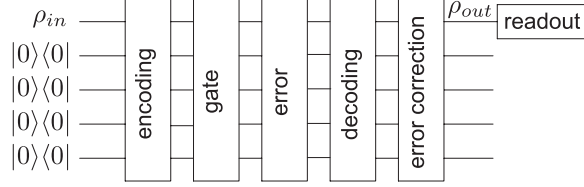


FIG. 1: Outline of the quantum algorithm.

Introduction.—Quantum computers can solve certain problems exponentially faster than classical computers [1, 2]. An essential precondition for realizing this potential is the preservation of the coherence between quantum states. This requirement makes the implementation of quantum computing much more challenging than for classical devices. Reliable quantum computing [3] is possible, in principle, provided quantum error correction (QEC) schemes can be implemented with a fidelity above a certain threshold [1, 4–7]. Every QEC code has an overhead in terms of gate operations and additional (ancilla) qubits. The protection of a single qubit against arbitrary single-qubit errors requires at least five physical qubits [8, 9]. Over the last few years, a series of experiments were performed that demonstrated that QEC is indeed capable of protecting quantum states against generated (artificial) errors or decoherence induced by the environment (see, e.g. [10–14]). However, the realization of reliable quantum computing requires more than the preservation of information: it must also be possible to process the encoded information by applying logical gate operations to the protected qubits. Here, we present an experimental demonstration of such gate operations on an encoded qubit. For encoding, we use a five bit QEC code [8, 9] that allows correction of arbitrary single-qubit errors (a so-called perfect QEC code) and demonstrate successful gate implementation and error correction. The result is a fault-tolerant implementation of the corresponding gate operations. Fig. 1 summarizes the scheme: it starts with encoding the input state of the first qubit into five physical qubits. To the resulting state, we apply one of three single-qubit gates - the identity, NOT or the Hadamard gate. As the third step, we apply another operation, which is either the identity (corresponding to no error) or one of the fifteen possible single-qubit errors. In the fourth step, the information is decoded, i.e. the output is extracted into the state of the first physical qubit. In the fifth and final step, possible errors are detected and corrected.

For the physical qubits, we use a system of five nuclear spins. The molecule containing the spins is dissolved in an anisotropic solvent. The resulting magnetic dipole couplings

between the nuclear spins are significantly stronger than the more frequently used scalar couplings and therefore result in a speedup of the gate operations by approximately an order of magnitude. The complete operation can therefore be completed within a time period significantly shorter than the coherence time of the system.

Five-qubit error correcting code.– Fig. 2 shows the quantum circuit for the five-qubit QEC code [8]. Qubit 1 is the register bit carrying the input state $|\varphi\rangle = \alpha|0\rangle + \beta|1\rangle$, where α and β are arbitrary complex numbers with $|\alpha|^2 + |\beta|^2 = 1$. The other four qubits are initialized in the state $|0\rangle^{\otimes 4}$. The unitary operation U_{en} implemented by the circuit encodes the state $|\varphi\rangle$ into a logical state as

$$U_{en}(\alpha|0\rangle + \beta|1\rangle)|0000\rangle = \alpha|0\rangle_L + \beta|1\rangle_L, \quad (1)$$

where

$$\begin{aligned} |0\rangle_L \equiv & \frac{1}{\sqrt{8}}(|00000\rangle - |10111\rangle - |01011\rangle + |11100\rangle \\ & + |10010\rangle + |00101\rangle + |11001\rangle + |01110\rangle) \end{aligned} \quad (2)$$

$$\begin{aligned} |1\rangle_L \equiv & \frac{1}{\sqrt{8}}(|11111\rangle - |01000\rangle + |10100\rangle - |00011\rangle \\ & + |01101\rangle + |11010\rangle - |00110\rangle - |10001\rangle) \end{aligned} \quad (3)$$

are the computational basis states of the logical qubit. The decoding operation U_{de} is the inverse operation of U_{en} , i.e., $U_{de} = U_{en}^\dagger$.

The five-qubit QEC code can detect and correct arbitrary single-qubit errors. The possible single-qubit errors for a five-qubit system can be written as bit flip errors Bk , phase flip errors Sk and combined bit- and phase flip errors BSk , where $k = 1 \dots 5$ indicates the affected qubit. These fifteen errors, together with the identity operation E define the possible outcomes if only single-qubit errors occur. The 2^4 possible states of the four syndrome qubits can distinguish between these 16 different outcomes. This is used by the error correction step, which is a unitary operation on the first qubit, controlled by all four syndrome qubits. Without the encoded gate operations, this code was implemented previously in a system of weakly coupled spin qubits [11].

Experimental protocol.–For the experimental implementation, we used the two fluorine and three proton spins of the molecule of 1,2-difluoro-4-iodobenzene, whose structure is shown in Fig. 3. The molecule was dissolved in the liquid-crystal solvent ZLI-1132 to retain the

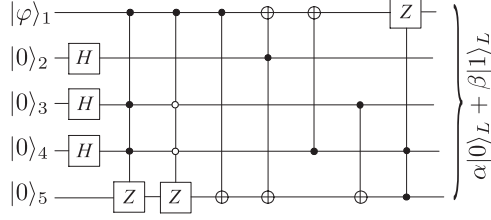


FIG. 2: Network representation of the encoding operation. The input state $|\varphi\rangle = \alpha|0\rangle + \beta|1\rangle$ is initially encoded in qubit 1. Qubits 2–5 are the syndrome bits. H denotes a Hadamard transform, and Z the π phase gate. The box or \oplus with a connected vertical line indicate controlled gates, where the filled or empty circle marks the control qubit. The operations are conditional on the control qubit being in state $|1\rangle$ (filled circle) or $|0\rangle$ (empty circle), respectively. The output of the circuit is the five-qubit state $\alpha|0\rangle_L + \beta|1\rangle_L$.

	F1	F2	H1	H2	H3
F1	2634.4	-227.7	-295.1	-610.5	-332.5
F2		-1630.5	-2221.9	50.6	-59.4
H1			126.8	-38.2	57.6
H2				-38.8	-2635.6
H3					42.9
$T_2^*(s)$	0.10	0.10	0.076	0.19	0.079

FIG. 3: Parameters of the spin qubits in the molecule 1,2-difluoro-4-iodobenzene. The inset shows the structure, where the five qubits 1–5 are spins F1, F2, H1, H2, and H3, respectively. The chemical shifts with respect to the transmitter frequencies of the proton and fluorine spins are shown as the diagonal terms and the dipolar couplings between spins are shown as the off-diagonal terms in units of Hz. The effective relaxation times T_2^* are determined by fitting the peaks in the spectra.

dipolar couplings between the spins. We denote the two fluorine spins F1 and F2 and the three protons H1, H2, and H3 as qubits 1–5. Data were taken with a Bruker Avance II 500 MHz spectrometer. The relevant Hamiltonian of the dipolar coupled spin system is, in frequency units, $\mathcal{H} = \sum_i \mathcal{H}_i^c + \sum_{i<j} \mathcal{H}_{ij}^d$, where $\mathcal{H}_i^c = \pi\nu_i Z_i$ is the Zeeman Hamiltonian and

$\mathcal{H}_{ij}^d = \pi D_{ij} Z_i Z_j$ describes the dipolar coupling Hamiltonian for the heteronuclear spins i and j , or $\mathcal{H}_{ij}^d = (\pi D_{ij}/2)(2Z_i Z_j - X_i X_j - Y_i Y_j)$ for the homonuclear case. The indices i and j run over all five spins, X_i , Y_i , Z_i denote the Pauli matrices, ν_i the chemical shift of spin i , and D_{ij} the coupling constant. Compared to the dipolar couplings, the scalar couplings between the spins are negligibly small or can be merged in the dipolar couplings [15]. To determine the numerical values of the Hamiltonian parameters, we measured different experimental spectra, using multiple quantum NMR [16] and heteronuclear decoupling. These spectra were used in a fitting process which yielded the parameters listed in Fig. 3.

We prepared the initial states $X\mathbf{0000}$ or $Y\mathbf{0000}$, with $\mathbf{0} \equiv |0\rangle\langle 0|$ by the circuit in Ref. [17]. The required unitary operations were implemented by two optimized shaped pulses designed with a GRAPE algorithm [15, 18, 19]. The experimental spectrum of the state $X\mathbf{0000}$ is illustrated in the Supplementary Material [15]. It contains a single main peak, which is the signature of a pseudopure state (PPS) [17]. By comparing with a reference spectrum obtained from the thermal state, we estimate that the polarization of this state is ≈ 0.72 of the maximum polarization that could result from an ideal preparation. For the following experiments, we normalized the spectra to this one, so the fidelities of the QEC protocol do not include losses during the PPS preparation [15]. The $Z\mathbf{0000}$ state was prepared by applying an additional $\pi/2$ rotation to the $X\mathbf{0000}$ state. After the encoding step, we applied one of the following gate operations to the logical qubit: the identity E , the NOT gate (up to a known phase), or the Hadamard gate.

The NOT gate N_L for the logical qubit is relatively simple to implement for this code, since it is transversal, i.e. it can be written as

$$N_L = R^y(\pi)^{\otimes 5}, \quad (4)$$

where $R^y(\pi) = e^{-i\pi Y/2}$. This relation can be verified by comparing the definitions of the logical states in Eqs. (2-3). The elements of N_L in the logical basis are represented as $\langle 0_L | N_L | 0_L \rangle = \langle 1_L | N_L | 1_L \rangle = 0$, $\langle 1_L | N_L | 0_L \rangle = i$, and $\langle 0_L | N_L | 1_L \rangle = -i$.

In contrast to the NOT gate, the Hadamard gate is not transversal in this code [20]. We therefore have to design an operation that implements this gate in the 2^5 dimensional Hilbert space of the five-qubit system. In this space, the Hadamard gate should generate a π rotation around the $(1,0,1)$ axis of the two-dimensional subspace spanned by the states $|0\rangle_L$ and $|1\rangle_L$ and an identity operation on the other 30 states. The corresponding unitary operator thus

has the matrix representation

$$H_L = \begin{pmatrix} \frac{1}{\sqrt{2}} & \frac{1}{\sqrt{2}} & & & \\ \frac{1}{\sqrt{2}} & -\frac{1}{\sqrt{2}} & & & \\ & & 1 & & \\ & & & \ddots & \\ & & & & 1 \end{pmatrix}, \quad (5)$$

where zero elements are not shown. This unitary operation can again be implemented by an optimized shaped pulse, designed in the same way as the other pulses described above. After the unitary gate operation, we also applied Bk , BSk , or Sk errors to the individual qubits, using single-qubit π rotations around the x , y , or z -axis.

For a quantitative evaluation of the algorithm's performance, we used quantum process tomography (QPT) [21] of the complete algorithm represented in Fig. 1. The process can be completely characterized by its χ matrix [1], which maps an arbitrary input state ρ_{in} into the output state $\rho_{out} = \sum_{kl} \chi_{kl} e_k \rho_{in} e_l^\dagger$. Here the operators $e_{k,l} \in \{E, X, -iY, Z\}$ denote the basis set for describing the process, and the indices $k, l = 1, \dots, 4$ run over the elements of the basis set. The measurement of χ requires the preparation of four input states $\rho_{in} = E, X, Y$, and Z . For each ρ_{in} , we determined the output state ρ_{out} by quantum state tomography. Since the unit operator E is always time-independent, the corresponding input state is omitted, assuming the output state is E . The quantum state tomography is performed by measuring in one experiment the transverse magnetization and in a second experiment applying a $\pi/2$ readout pulse and then measuring the transverse magnetization. The measured FIDs were Fourier transformed and the resulting spectra were fitted to the theoretical spectra by adjusting as a single parameter the overall amplitude. Having the output states for the four input states, we determined the χ matrix using the established strategy [1]. For each process, we quantified the performance by comparing the experimental (χ_{exp}) and theoretical (χ_{th}) χ matrices via the fidelity [22]

$$F_\chi = |\text{Tr}(\chi_{exp} \chi_{th}^\dagger)| / \sqrt{\text{Tr}(\chi_{exp} \chi_{exp}^\dagger) \text{Tr}(\chi_{th} \chi_{th}^\dagger)}. \quad (6)$$

Experimental results.—We first checked the encoding, encoded gate and decoding operations with a simplified experimental scheme. Compared to the full scheme shown in Fig. 1, we omitted the error and error correction operations. Fig. 4 shows the experimental

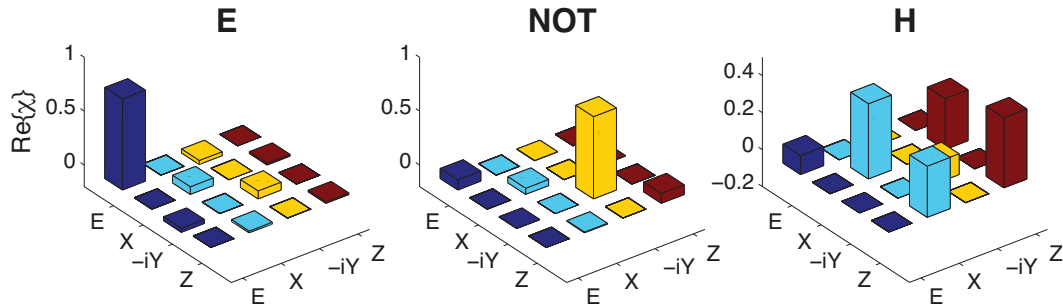


FIG. 4: Bar plots of the real parts of the χ matrices for the identity, NOT and Hadamard gates in logical states. The RMS values of the imaginary parts are 0.035, 0.0069, and 0.017, respectively.

results for the process matrices χ as bar plots. The corresponding matrices for the ideal operations have $\chi_{11} = 1$ for the identity operation, $\chi_{33} = 1$ for the NOT operation, and $\chi_{22} = \chi_{44} = \chi_{24} = \chi_{42} = 0.5$ for the Hadamard gate. All other elements should vanish. We find a good qualitative agreement between the theoretical and experimental values, with fidelities of 0.979, 0.983, and 0.956, for the identity, NOT and Hadamard gates, respectively. We next tested the full implementation, including errors and error correction. Fig. 5 illustrates the results for three out of 48 experiments. In the first example (trace b), we initialized the system to the Y state and applied an E gate and S1 error operation, followed by the decoding and error correction steps. Trace c) shows the corresponding results for the X initial state, NOT gate and BS4 error and d) for Z initial state, H gate and B5 error. The insets show enlarged partial spectra containing the main signal components, with the experimental spectra represented by dashed lines, the ideal spectra as full lines. Experimental and theoretical curves were both normalized to the spectra of the initial PPS. Figure 6 shows the measured fidelities for each of the 48 different experiments as a bar plot. The solid horizontal line shows the average fidelity for each type of gate, averaged over the 16 different error conditions.

To assess the usefulness of the scheme, we compare the achieved fidelities to an idealized experiment where we do not use QEC, but the same 16 error conditions can occur, with equal probabilities. In this case, the three single qubit errors acting on the first qubit result in zero fidelity, while the other 13 error conditions (the identity and the single-qubit errors on the ancilla qubits) result in fidelities of one. Averaged over these 16 reference experiments, we would thus expect an average fidelity of $13/16 = 0.8125$. This value is shown in the figure

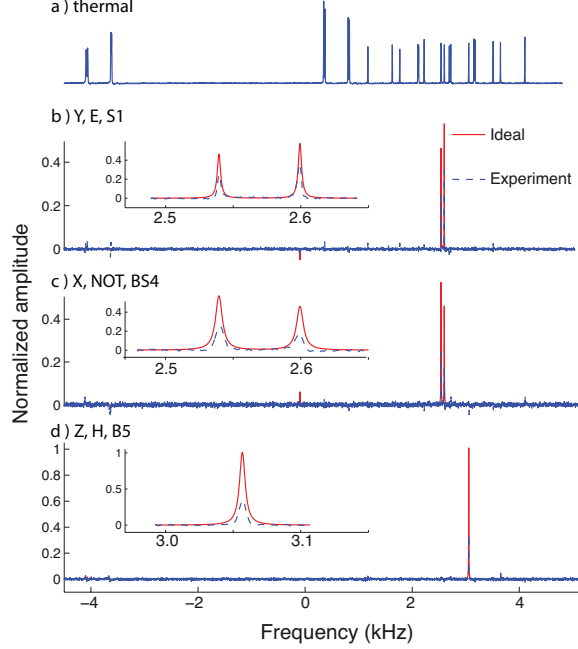


FIG. 5: (Color online.) Spectra of the fluorine spins obtained for different versions of the experiment. a) Reference spectrum obtained by applying a $\pi/2$ pulse to the thermal equilibrium state. b) Spectrum of the output state, starting with the initial state Y , encoding, applying the identity operation, S1 error and error correction. c) Same as b), but $\rho_{in} = X$, NOT gate and BS4 error. d) Same as b), but $\rho_{in} = Z$, Hadamard gate and B5 error. The dashed and solid curves indicate the experimental and simulated spectra, which are normalized to the initial pseudopure states. The lines with the main signal contributions are shown enlarged as insets.

as the horizontal dashed line. The average fidelity for the three different gates exceeds this reference value by 0.0837, 0.0528 and 0.0196, for the identity, NOT and Hadamard gates, respectively. This shows that the performance of the QEC scheme is high enough to compensate the additional errors affecting the syndrome qubits as well as the errors due to experimental imperfections of the encoding, decoding and error correction steps.

Discussion.—The fidelities achieved in these demonstration experiments are still lower than the threshold fidelities required for scalable quantum computation. We have identified four main causes for the observed reduction of fidelity: (i) Stability and homogeneity of the magnetic and radio frequency (r.f.) fields were less than ideal, since the lack of deuterium in the sample did not allow operation of the lock system of the spectrometer. (ii) Finite accuracy of the Hamiltonian parameters. (iii) Finite coherence time: the duration of the

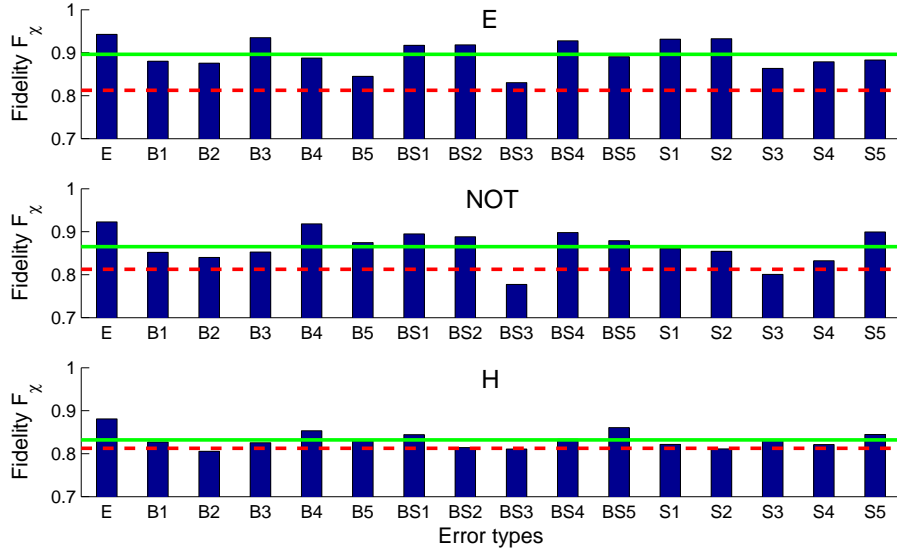


FIG. 6: Bar plots showing the experimentally determined fidelities for the identity, NOT and Hadamard gates applied to the encoded qubit after applying error operations and error correction. The average fidelity is shown as the solid line. Compared to the average fidelity without error correction, shown as the dashed line, the encoding - decoding - error correction scheme improves the fidelity.

experiment is in the range of 26–64 ms (excluding the preparation of the initial PPS), which is comparable to the measured T_2^* . (iv) Deviations between the calculated pulse shapes and those acting on the spins, which are caused mostly by nonlinearities of the spectrometer hardware. Our efforts to suppress these imperfections concentrated on 1) using short gate durations, 2) designing the pulses robust to variations of the r.f. strength and insensitive to frequency offsets and 3) ‘fixing’ the pulses by measuring the actual amplitudes of the control gates with a pick up coil and adjusting the amplitudes to minimize the difference between theoretical and experimental values [23].

For a better understanding of the sources of errors, we performed a quantitative analysis of one of the experiments: the Hadamard gate combined with a phase flip error at qubit 5 and the corresponding error correction [15]. Combining experimental results and simulation, we estimate that the field inhomogeneity and the imperfect implementation of the pulses contribute ≈ 0.09 to the loss of fidelity. Additionally the limit of T_2 and the imprecision in characterizing the Hamiltonian, contribute ≈ 0.04 and 0.03 to the loss of fidelity, respectively.

The simulation with T_2^* results in a fidelity below the experimental value, indicating that the coherence time in the experiment is longer than T_2^* . This is expected if the gate operations refocus some of the inhomogeneity of the system.

Conclusion.—The results presented here are a first demonstration of one of the most important preconditions for reliable quantum computation: the implementation of logical gate operations on encoded qubits. While QEC has been demonstrated on quantum memories, its combination with *processing* of quantum information is an important milestone towards the implementation of reliable quantum computing. The present demonstration used three single-qubit gate operations acting on a logical qubit encoded in a perfect five-qubit QEC code. In the earlier implementation of this code [11], without the gate operations, the experimental duration was > 300 ms. Compared to that, we have reduced the duration of the experiment by approximately one order of magnitude by using a dipolar coupled system, whose interactions are stronger than the scalar couplings used before. The reduction of the gate operation times opened the possibility to implement in addition the logical gate operations. With better homogeneity and more precise Hamiltonian parameters, it should be possible to improve the experimental fidelity. The recent theoretical progress in measuring Hamiltonians with dipolar couplings [24] and optimal algorithms in pulse finding [25] should be helpful for this purpose. This will allow us to control larger systems, encoding multiple qubits and implementing multi-qubit gate operations, such as CNOT in the encoded qubits. If the fidelity can be improved sufficiently to reach the error threshold, the combination of QEC with logical gate operations will pave the way to reliable quantum computation.

Acknowledgments.—The authors acknowledge A. M. Souza, B. Zeng, M. Grassl, D. A. Trotter, and V. J. Villanueva for helpful discussions, and M. Holbach and J. Lambert for help in experiment. This work is supported by the Alexander von Humboldt Foundation, and the DFG through Su 192/19-1.

-
- [1] M. Nielsen and I. Chuang, *Quantum Computation and Quantum Information* (Cambridge University Press, Cambridge, 2000).
 - [2] J. Stolze and D. Suter, *Quantum Computing: A Short Course from Theory to Experiment* (Wiley-VCH, Berlin, 2nd edition, 2008).

- [3] J. Preskill, Proc. R. Soc. Lond. A **454**, 385 (1998).
- [4] E. Knill, Nature, **434**, 39 (2005).
- [5] D. Gottesman, *Encyclopedia of Mathematical Physics*, edited by J.-P. Francoise, G. L. Naber, and S. T. Tsou, 196, Elsevier, Oxford, (2006).
- [6] D. Gottesman, quant-ph/9705052, Caltech Ph.D. thesis.
- [7] P. Aliferis, D. Gottesman, and J. Preskill, Quantum Information and Computation, **8**, 0181 (2008).
- [8] R. Laflamme et al., Phys. Rev. Lett. **77**, 198 (1996).
- [9] C. H. Bennett et al., Phys. Rev. A **54** 3824 (1996).
- [10] D. G. Cory et al., Phys. Rev. Lett. **81**, 2152 (1998).
- [11] E. Knill et al., Phys. Rev. Lett. **86**, 5811 (2001).
- [12] O. Moussa et al., Phys. Rev. Lett. **107**, 160501 (2011).
- [13] J. Chiaverini et al., Nature **432**, 602 (2004).
- [14] M. D. Reed et al., Nature **482**, 382 (2012).
- [15] See supplemental material for details regarding (1) designing the unitary operations for error correction, (2) results for measuring the parameters of the spins, (3) quantum circuit for preparing the pseudopure state and spectra obtained in experiment and by simulation, and (4) experimental error analysis.
- [16] B. Baishya and N. Suryaprakasha, J. Chem. Phys. **127**, 214510 (2007).
- [17] E. Knill et al., Nature **404**, 368 (2000).
- [18] N. Khaneja et al., J. Magn. Reson. **172**, 296 (2005).
- [19] C. A. Ryan et al., Phys. Rev. A **78**, 012328 (2008).
- [20] B. Zeng, A. W. Cross, and I. L. Chuang, IEEE Trans. Inf. Theory, **57**, 6272, (2011).
- [21] I. L. Chuang and M. A. Nielsen, J. Mod. Opt. **44**, 2455 (1997); J. F. Poyatos, J. I. Cirac and P. Zoller, Phys. Rev. Lett. **78**, 390 (1997).
- [22] X. Wang, C.-S. Yu, and X. Yi, Phys. Lett. A **373**, 58 (2008).
- [23] C. A. Ryan, M. Laforest, and R. Laflamme, New J. Phys. **11**, 013034 (2009).
- [24] W. Leo Meerts et al., J. Chem. Phys. **130**, 044504 (2009); D.-A. Trottier, V.J. Villanueva, J. Zhang, M. Ditty, and R. Laflamme (to be published).
- [25] P. de Fouquieres, Phys. Rev. Lett. **108**, 110504 (2012).